sustainability

MDPI

Article

Oleic Acid-Tailored Geopolymer Microspheres with Tunable Porous Structure for Enhanced Removal from Tetracycline in Saline Water

Xiaoyun Wang, Zheng Zhang and Yuanyuan Ge *

School of Chemistry & Chemical Engineering, Guangxi Key Lab of Petrochemical Resource Processing and Process Intensification Technology, Guangxi University, Nanning 530004, China; 18166592844@163.com (X.W.); zhangz0282@163.com (Z.Z.)

* Correspondence: geyy@gxu.edu.cn

Abstract: Tetracycline (TC) in the water body poses a huge threat to the ecological environment. There is a great challenge to develop highly efficient, green, low-cost and reusable adsorbents for TC removal from saline water. Herein, metakaolin-based geopolymer microspheres (MM) modified by oleic acid were proposed for the enhanced adsorption of TC from saline water. Experimental and characterization results showed that the introduction of oleic acid into the MM effectively adjusted the specific surface area, pore volume and zeta potential of the MM, thus accelerating the adsorption rate and enhancing the TC adsorption capacity of the MM. The adsorption process fitted well to the pseudo-second-order kinetic and Langmuir isothermal models. The Langmuir adsorption capacity of TC by the optimal MM, namely MM3 (0.3%, oleic acid), reached 645.7 $mg \cdot g^{-1}$ at 298 K, which was higher than many reported adsorbents. The adsorption process was endothermic and spontaneous. The MM3 had good adsorption performance of TC from saline water and regeneration performance. Moreover, the breakthrough curves of the MM3 in a column system were correlative with the Thomas and Yoon–Nelson models. The adsorption mechanisms of TC by the MM3 involved Van der Waals forces, electrostatic interactions, hydrogen–bonding interactions, and ion exchange.

Keywords: oleic acid; geopolymer microspheres; adsorption; tetracycline

Citation: Wang, X.; Zhang, Z.; Ge, Y. Oleic Acid-Tailored Geopolymer Microspheres with Tunable Porous Structure for Enhanced Removal from Tetracycline in Saline Water. *Sustainability* **2022**, *14*, 6705. https://doi.org/10.3390/su14116705

Academic Editor: Vincenzo Torretta

Received: 18 April 2022
Accepted: 17 May 2022
Published: 30 May 2022

1. Introduction

As a widely used antibiotic drug for curing diseases, tetracycline (TC) has been frequently detected in sewage treatment plants, hospital wastewater, natural rivers, harbors and lakes [1–3]. The accumulation of TC in the environment puts tremendous pressure on the ecological balance, for example, by producing super-resistant bacteria [3,4].

Many technologies have been reported for TC removal from aqueous solutions such as adsorption, membrane filtration, biodegradation, advanced oxidation processes (AOPs), etc., [5–7]. The biodegradation method is environmentally friendly and low in cost but requires a large area and requires high water quality [6]. AOPs have the advantages of simple operation, strong oxidative ability and environmental friendliness, but the cost of degrading pollutants by this method is very expensive. Moreover, the biodegradation method and AOPs are also limited by the production of toxic intermediates [6,7]. Membrane processes are simple to operate and have low energy consumption, but membrane-fouling issues limit the application of membranes [5]. Adsorption is a method of removing pollutants from wastewater by transferring pollutants from the liquid phase to the surface of the solid phase, and the adsorption method stands out owing to its high removal efficiency and convenient operation [8,9], including with activated carbons [10,11], metal oxides [12], composites [13,14], modified metal–organic frameworks (MOFs) [15,16], etc., [17,18]. However, the above adsorbents are limited in further application due to their powder form, which, in practical application, is difficult to recover to continue the treatment of wastewater.

As an emerging, environmentally benign material, geopolymers are made from silicon and aluminum-rich materials (e.g., fly ash, metakaolin and slag) under alkaline conditions and have the advantages of chemical and mechanical stability, low cost, simple preparation and three-dimensional structure [19–22]. Geopolymers contain negatively charged aluminum oxide tetrahedrons $[AlO_4]^-$, which can adsorb heavy metals and dyes through electrostatic attraction and ion-exchange [23–30]. The good molding and processing properties allow geopolymers to be processed into spherical particles on different scales, which facilitates their recovery and filling into fixed beds for continuous wastewater treatment. Tang et al. reported that the adsorption capacity of Cu^{2+}, Pb^{2+} and Ca^{2+} by geopolymer microspheres was 34.5, 45.1 and 24 $mg \cdot g^{-1}$, respectively, and the equilibrium time (t_e) of the three metal ions was about 36 h [31]. In another study, Papa et al. prepared ice-templated geopolymer beads to adsorb methylene blue [32]. The above studies explored the prospects of geopolymers for heavy metal and dye removal. However, to date, studies related to the application of geopolymers for the adsorption of TC from saline water have not been reported and the abovementioned geopolymer-based adsorbents still have disadvantages such as slow mass transfer rates and low adsorption capacity.

In this study, metakaolin-based geopolymer microspheres (MM) with tunable porous structures and surface properties were newly proposed for efficient removal of TC from saline water. To achieve this goal, oleic acid, a mono-unsaturated fatty acid used widely in vegetable oils, was used as a modifier for the preparation of the MM. Oleic acid can neutralize excess alkali, regulate the pH level during geopolymerization, control the dissolution of aluminum in metakaolin and the $[AlO_4]^-$ content in the resultant geopolymer framework, thus modulating the surface charges of the geopolymer. In addition, the as-formed sodium oleate can act as a surfactant to improve the viscosity of the slurry and also stabilize the formed bubbles, thus adjusting the pore structure of geopolymer and increasing its surface area and pore volume, which reduces the mass transfer resistance in the adsorption process and accelerates the response rate [33]. Moreover, TC usually coexists with inorganic salts (e.g., NaCl and Na_2SO_4) in real wastewater or seawater [34], which requires the adsorbent to have good salt tolerance. Metakaolin-based geopolymer presents good durability in seawater [35] and is thus very conducive to treating TC from saline water. Therefore, this study was proposed to explore (1) the effect of oleic acid on the structure and properties of the MM; (2) the adsorption kinetics, thermodynamics and the adsorption mechanism of the MM for TC; (3) the applicability of MM to the removal TC from saline water; (4) the continuous treatment performance of TC aqueous solution in a fixed-bed column; and (5) the regeneration and reusability of the MM.

2. Experimental Section

2.1. Materials and Reagents

Industrial sodium silicate ($n(SiO_2)/n(Na_2O)$ = 3.14, wt.%(SiO_2) = 25.99%, wt.% (Na_2O) = 8.60%, wt.%(H_2O) = 62.48%) and metakaolin (wt.%(SiO_2) = 51.02%, wt.% (Al_2O_3) = 51.02%, wt.%(Na_2O) = 0.18%) were purchased from Nanning Chunxu Chemical Co., Ltd. (Nanning, China) and Chaopai New Materials Co., Ltd. (Nei Mongol, China) Polyethylene glycol 2000 (PEG-2000, 99%), tetracycline (TC, 99.5%) and oleic acid (99%) were obtained from Mclean Biochemical Technolog Co., Ltd. (Shanghai China) Sodium hydroxide (NaOH, 96%) was purchased from GHTECH Co., Ltd. (Shantou, China) Hydrochloric acid (HCl, 36.5%) was obtained from Chron Chemical Co., Ltd. (Chengdu, China).

2.2. Preparation of MM

Metakaolin-based geopolymer microspheres (MM) were formed as shown in Figure 1, according to the published literature [36]. Briefly, metakaolin (15 g), waterglass with $n(SiO_2)/n(Na_2O)$ = 1.5 (30.84 g), deionized water (6.19 g) and oleic acid (0–0.5 wt%) were added into a plastic beaker to prepare a slurry. Then, the slurry was injected into 800 mL PEG-2000 of 80 °C at the rate of 1 drop/s and was evenly dispersed in PEG-2000 to solidify

with continuous stirring. After curing, washing and drying, MMx (x represents the mass ratio of oleic acid in the geopolymer slurry) was obtained.

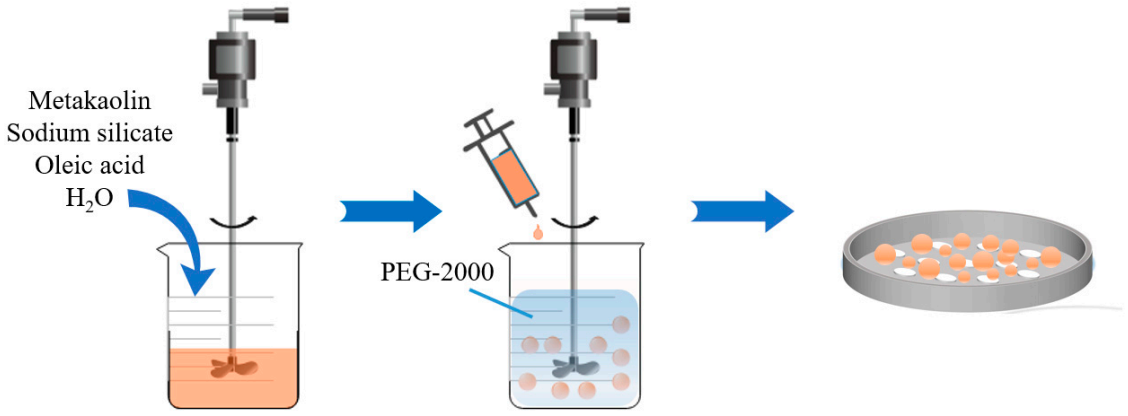

Figure 1. Schematic representation of MM.

2.3. Characterizations

The morphologies of MM were observed by a scanning electron microscope (SEM, S-3400 N, Hitachi Co., Ltd., Tokyo, Japan). An X-ray diffractometer (XRD, MiniFlex600, Science Co., Ltd., Tokyo, Japan) was recorded to analyze the crystal phase. X-ray photoelectron spectroscopy (XPS, Thermo ESCALAB 250Xi, Thermo Fisher Scientific, Waltham, MA, USA) was conducted to determine elemental properties of the samples. Fourier transform infrared spectroscopy (FT-IF, Nicolet iS50, Thermo Fisher Scientific, Waltham, MA, USA) was employed to analyze surface functional groups. Zeta potential was measured at different pH levels with a zeta potential analyzer (NanoBrook Omni, Brookhaven Instruments Co., Ltd., Holtsville, NY, USA). The pore-size distribution and specific surface area of samples were measured in N2 adsorption–desorption analysis (Gemini VII 2390, Micromeritics, Norcross, GA, USA). All sample characterizations were performed 3 times.

2.4. Batchwise Adsorption

Different doses of MM were dispersed into varying concentrations of TC aqueous solutions at different pH levels and different contact times to test the application performance of the adsorbent. Prepared 1 mol·L^{-1} NaOH or 1 mol·L^{-1} HCl was added to regulate the pH of the aqueous solution. Blank experiments were conducted to eliminate the irrelevant effects. The adsorption solution was filtered with a 22 μm syringe-driven filter, and the concentration of TC was determined by high performance liquid chromatography (HPLC) with mobile phase of acetonitrile/acetic acid (25:75, *V*/*V*). The equilibrium adsorption capacity (Q_e, mg·g^{-1}) and removal efficiency (R, %) of TC were calculated using Equations (1) and (2):

$$Q_e = \frac{V(C_0 - C_e)}{m} \quad (1)$$

$$R(\%) = \frac{C_0 - C_e}{C_0} \times 100\% \quad (2)$$

where V (L) is the volume of added aqueous solution, C_0 (mg·L^{-1}) is the initial concentration of tetracycline, C_e (mg·L^{-1}) is the final concentration of tetracycline after being adsorbed and m (g) is the mass of added adsorbent. All experiments were performed 3 times, and the average value was taken as the final result.

2.5. Fixed-Bed Column Experiments

MM3 was filled into a fixed-bed (0.5 cm internal diameter) and its continuous processing TC performance was evaluated through the breakthrough curve. The TC solution (C_0 = 250 mg·L^{-1}, pH = 4, T = 298 K) was pumped into fixed-bed with a flow rate of 1 mL·min^{-1}.

The effects of bed heights (0.06 g MM3 was required to fill the column per cm) on the removal efficiency of TC by MM3 were investigated. The Thomas model and Yoon–Nelson model were fitted to reflect the kinetics of fixed-bed adsorption system of TC by MM3. The linear form of each model is as follows [37]:

Thomas model:

$$\ln\left(\frac{c_0}{c_t}-1\right)=\frac{k_{th}Q_f m}{q}-k_{th}c_0 t \quad (3)$$

Yoon–Nelson model:

$$\ln\left(\frac{c_t}{c_0-c_t}\right)=k_{yn}t-\tau k_{yn} \quad (4)$$

where c_t is the TC concentration flowing out of the fixed bed, mg·L^{-1}; Q_f is the maximum adsorption capacity, mg·g^{-1}; q is the flow rate of TC solution in the fixed bed, L·h^{-1}; k_{th} and k_{yn} represent the rate constants of Thomas and Yoon–Nelson models, respectively. τ is the breakthrough time when c_t/c_0 = 0.5, min.

The two models complement each other to analyze the kinetics of the penetration curve. Thomas model is mainly used to calculatethe maximum adsorption capacity, Q_f, and the adsorption rate constant, k_{th}, of the fixed bed. Yoon–Nelson model is mainly used for describing adsorption behavior or 50% adsorbent breakthrough time [38].

3. Results and Discussion

3.1. Fabrication of MM

To obtain optimal the MM, the effect of the oleic acid dosage on the adsorption performance of the MM was firstly investigated. In Figure 2a, as the dosage of oleic acid increased from 0.0% to 0.3%, the Q_e increased from 387 mg·g^{-1} to the maximum 445 mg·g^{-1}. It was because oleic acid can effectively increase the surface area of the MM after being converted in situ into surfactant in the alkaline system of the geopolymer (Table S1). The MM3 with the largest surface area (40.09 m^2·g^{-1}) and larger pore volume (0.15 cm^3·g^{-1}) provided more active sites for adsorption and had the highest Q_e. Excessive oleic acid results in a lower pH in the system and a unstable geopolymer gel structure, resulting in a lower specific surface area and lower Q_e [39]. In Figure 2b, the adsorption equilibrium times (t_e) of TC by the MM3 and MM0 were 360 min and 720 min, respectively. Compared with the MM0, the adsorption equilibrium time by MM3 was reduced by half. This indicates that adding oleic acid can effectively increase the adsorption capacity and adsorption rate of MM.

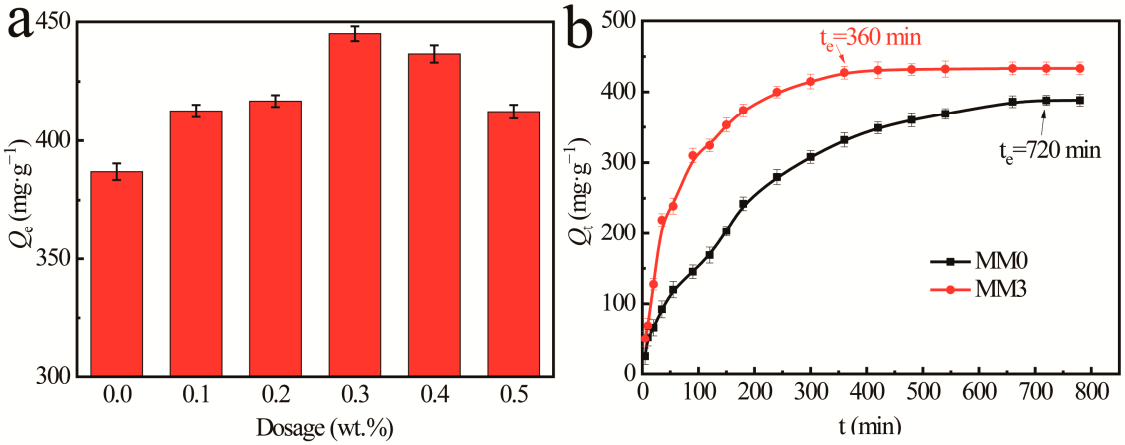

Figure 2. (**a**) Q_e of TC by MM with different dosages of oleic acid ($m_{adsorbent}$ = 0.01 g; V = 20 mL; C_0 = 250 mg·L^{-1}; pH = 4; T = 298 K; t = 12 h) and (**b**) the curve of adsorption kinetics of MM0 and MM3 ($m_{adsorbent}$ = 0.01 g; V = 20 mL; C_0 = 250 mg·L^{-1}; pH = 4; T = 298 K).

3.2. Characterization of MM

An SEM was used to observe the morphologies of MM0 (Figure 3a,b) and MM3 (Figure 3c,d). The surface of MM0 was comparatively smooth and dense, while the surface of MM3 was porous and loose, which could provide a larger surface area and more active sites for TC adsorption. MM3 and MM0 were typical geopolymeric amorphous structures, which was further confirmed by the XRD patterns (Figure 4a).

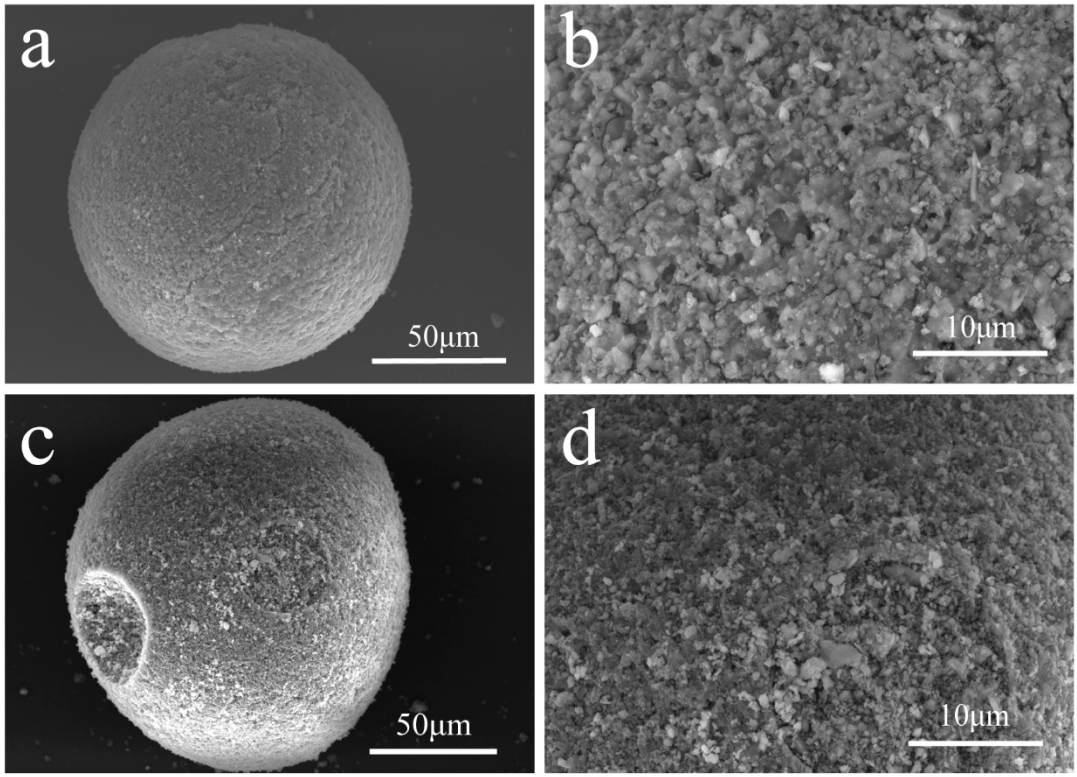

Figure 3. SEM photographs of MM0 (**a**,**b**) and MM3 (**c**,**d**).

A wide dispersion peak of 2θ = 22°–30°, which belonged to the characteristic peak of the geopolymer [36], was observed in both MM0 and MM3. Although the amorphous structure of the geopolymer was not changed, the center position of the dispersion peak was shifted from 26.7° in MM0 to 24.1° in MM3 due to the addition of the oleic acid. It might be because the oleic acid was converted in situ to surfactants encapsulated in the MM3.

As shown in Figure 4b of the FT-IR spectra, the strong adsorption peaks at 3452 cm^{-1} and 1636 cm^{-1} belonged to the O–H bonds from water [26]. The broad band around 1057 cm^{-1} corresponded to the asymmetric stretching vibration of the Si–O–T (T = Si and Al). The vibrations of Si–O–Si (878 cm^{-1}), Si–O–Al (709 cm^{-1} and 575 cm^{-1}) and O–Si–O (457 cm^{-1}) were observed in both MM0 and MM3 [24,25]. The new peak at 1466 cm^{-1}, which was attributed to –C=O/C–O of the oleic acid was appeared in MM3, indicating the successful introduction of oleic acid into the MM3 [40].

The pore-size distribution of the MM0 and MM3 was in the range of 10–180 nm, shown in Figure 4c. Total pore volume of the MM3 (0.15 $cm^3 \cdot g^{-1}$) was much larger than that of the MM0 (0.09 $cm^3 \cdot g^{-1}$) (Table 1), and the porosity values for the MM0 and MM3, as measured by the density bottle method, were 69.0% and 91.3%, respectively, which benefit the mass transfer. Specifically, the mesoporous volume of the MM3 (0.057 $cm^3 \cdot g^{-1}$) was about twice that of the MM0 (0.028 $cm^3 \cdot g^{-1}$), which facilitated the diffusion of the TC into the inner surface of the MM3 [41]. It confirmed that the introduction of oleic acid improved the pore structure of MM.

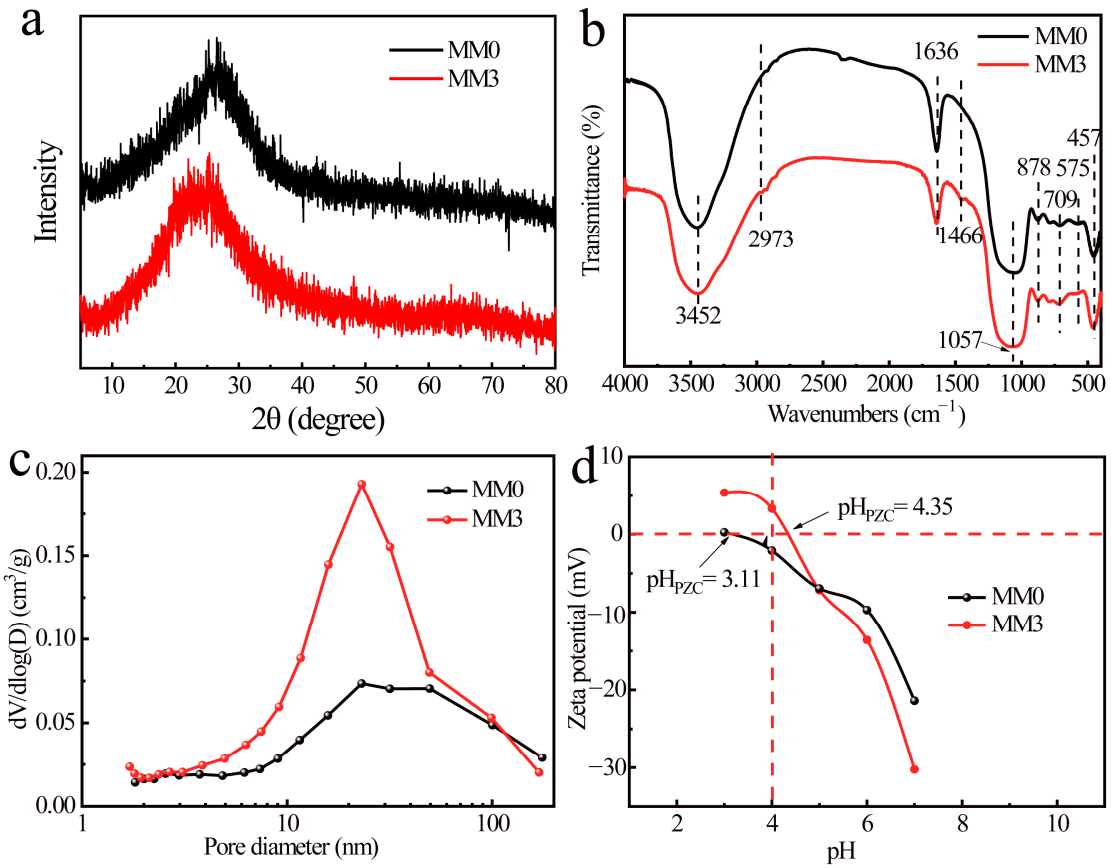

Figure 4. (**a**) XRD patterns, (**b**) FTIR spectra, (**c**) pore size distribution, and (**d**) zeta potential at different pH of MM0 and MM3.

Table 1. Pore-volume parameters of MM0 and MM3.

Adsorbent	BET-Specific Surface Area $m^2 \cdot g^{-1}$	Total Pore Volume $cm^3 \cdot g^{-1}$	Mesoporous Volume $cm^3 \cdot g^{-1}$	Macroporous Volume $cm^3 \cdot g^{-1}$
MM0	24.23	0.09	0.028	0.059
MM3	40.09	0.15	0.057	0.059

The zeta potential affects the adsorption performance and the zeta potential of the MM0 and MM3 is displayed in Figure 4d. It shows that the isoelectric points of the MM0 and MM3 were 3.11 and 4.53, respectively, indicating that the introduction of oleic acid was an effective way to adjust the zeta potential of the geopolymer.

3.3. Batchwise Adsorption Studies

3.3.1. Effects of Adsorbent Dosage and pH Value

Figure 5a shows the influence of the MM3 dosages on the *R* of TC. *R* increased from 70.06% to 86.47% with increasing MM3 dosages from 0.005 g to 0.01 g, which was attributed to larger adsorption area and a greater number of adsorption sites; more adsorbents could not increase *R*, which is consistent with the literature [42]. It should be noted that the Q_e of the TC was decreasing as the dosage of the MM3 was increasing, due to ineffectively utilized adsorption sites. Therefore, the optimal MM3 dosage was determined to be 0.01 g/20 mL for TC.

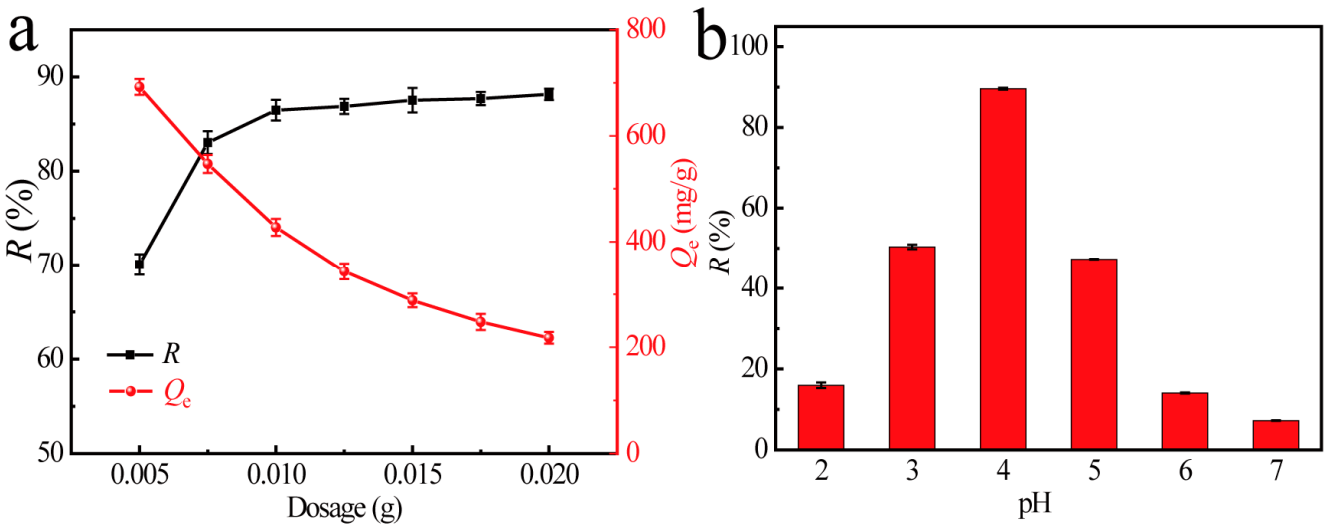

Figure 5. Effect of (**a**) MM3 dosage (pH = 4, C_0 = 250 mg·L^{-1}, V = 20 mL, T = 298 K; t = 12 h) and (**b**) pH value on the adsorption of TC by MM3 (m_{MM3} = 0.01 g, C_0 = 250 mg·L^{-1}, V = 20 mL, T = 298 K; t = 12 h).

The adsorption performance was greatly determined by the pH during the adsorption process, as shown in Figure 5b [10]. The R_{max} of the TC adsorbed by the MM was about 90% at pH = 4. When the pH value was not 4, the R by the MM3 was significantly reduced, even reaching 16.0% or 7.3% when the pH values were 2 or 7, which was because the pH value of the TC solution has an impact on the TC dissolution and the surface charges of the adsorbents. TC exists as a cationic TC^+, zwitterionic $TC^{+/-}$, net monoanionic $TC^{+/-}$, and two negatively charged anion TC^- species under pH < 3.3, 3.3 < pH < 7.68, 7.68 < pH < 9.69 and pH > 9.69, respectively [43]. As discussed in Section 3.2, the isoelectric point was 4.35, indicating that the MM3 was positively charged when the pH < 4.35, and the MM3 was negatively charged when the pH > 4.35. The positively charged MM and TC repelled each other, so the R was significantly reduced when the pH = 2 or 3 [44]. The zeta potential of the MM3 was negative when the pH > 4.35, indicating that the surface of the MM3 was negatively charged, which was caused by the negatively charged aluminum oxide tetrahedron $[AlO_4]^-$ in the geopolymer, and with the increasing of the pH, the zeta potential decreased. It was generally recognized that lower pH was favored for the adsorption of the TC by MM3 owing to the cation exchange of TC^+ with Na^+ of the MM3 [17].

3.3.2. Effect of Contact Time, TC Initial Concentration and Temperature

Contact time was a significant factor in the adsorption. In Figure 6a, Q_t increased evidently at the beginning, and then increased slowly with the contact time increasing until reaching adsorption equilibrium, which was likely due to the reduction in adsorption sites [9]. As C_0 of the TC solution increased from 100 to 400 mg·L^{-1}, t_e rose from 55 to 480 min. It can be seen in Figure 6b that the R reached 100% when C_0 was 50 mg·L^{-1}. The R decreased with incremental C_0, which was because the fixed active site of the MM3 was constantly occupied by the increase in pollutant concentration and excess TC could not be adsorbed. As C_0 rose from 50 to 500 mg·L^{-1}, the Q_e rose from 100 to 839.8 mg·g^{-1}. It was most likely that the number of adsorption sites was fixed, and the active site was insufficient to adsorb the TC molecule in the low concentration [45]. Moreover, Figure 6c shows that the maximal Q_e rose from 645.8 to 839.8 mg·g^{-1} with the increasing of the temperature from 298 to 318 K. It could be inferred that raising the temperature was favorable to adsorption, and more details are explained in the isotherm section.

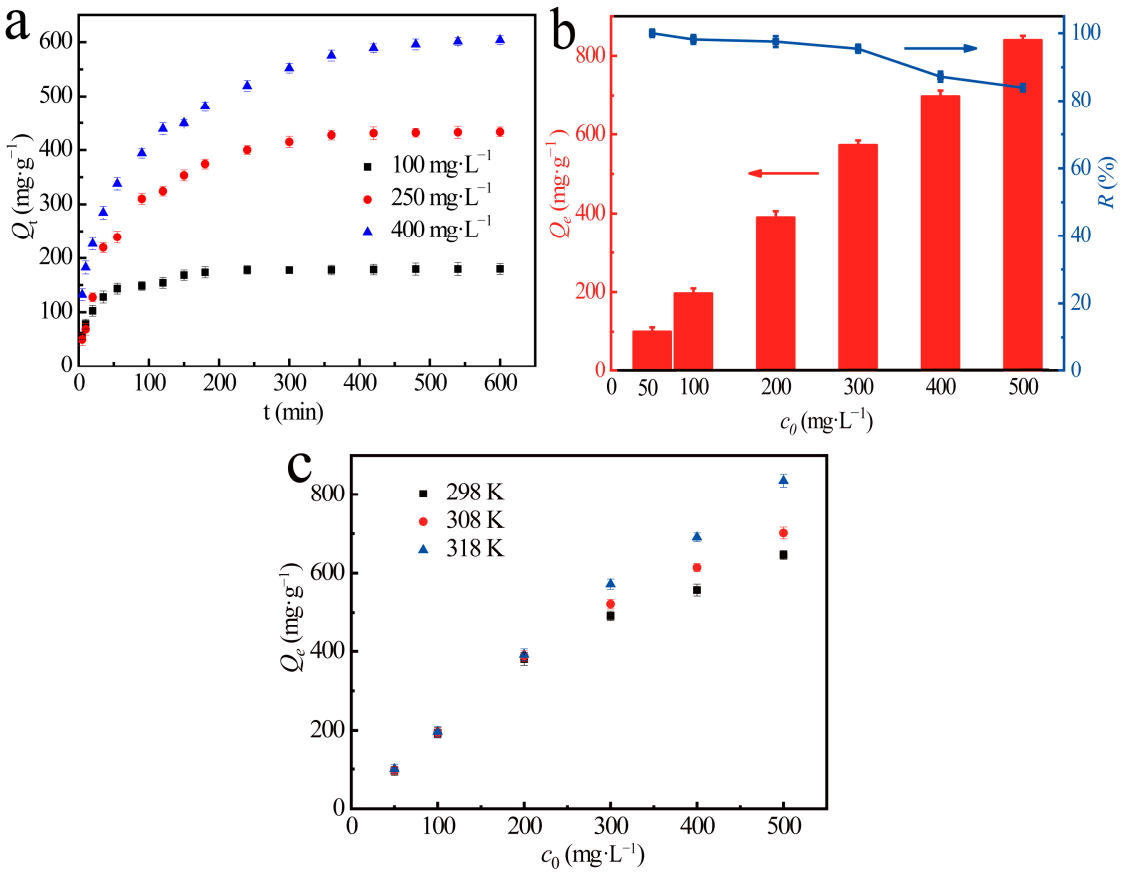

Figure 6. (**a**) Effect of time on the adsorption (m_{MM3} = 0.01 g; pH = 4; V = 20 mL; T = 298 K) and (**b**) TC initial concentration on Q_e of TC by MM3 (m_{MM3} = 0.01 g; pH = 4; V = 20 mL; t = 12 h; T = 318 K) and (**c**) Q_e of TC onto MM3 at different temperatures (m_{MM3} = 0.01 g; pH = 4; V = 20 mL; t = 12 h).

3.4. Adsorption Kinetics and Isotherms

The pseudo-first-order kinetic, pseudo-second-order kinetic and intra-particle diffusion models were used to fit the adsorption kinetic curve of TC by MM3 so as to elucidate the adsorption process. The equations of the three kinetic models [46] are presented in the Supplementary Materials (Equations (S1)–(S3)).

As can be seen in Figure 7 and Table 2, the correlation coefficients of the pseudo-second-order dynamics model of the different TC initial concentrations (R^2 = 0.996, 0.999, 0.993) were larger than those of the pseudo-first-order dynamics model (R^2 = 0.966, 0.992, 0.977), indicating that the adsorption of TC by MM3 was more in line with the pseudo-second-order kinetic model, which was consistent with what is reported in the literature [47]. The intra-particle diffusion model can be divided into three kinetic stages, including the liquid film diffusion, intra-particle diffusion and adsorption reaction stages, as shown in Figure 7 and Table 3. The intercept C was not 0, showing that intra-particle diffusion was not the only factor affecting the adsorption rate [48]. Moreover, the diffusion rate constants of the three stages in intra-particle diffusion were in descending order: $k_{i1} > k_{i2} > k_{i3}$, indicating that liquid film diffusion dominated the adsorption process of the TC by the MM3. k_i continued to increase with the increasing C_0 of the TC, indicating that the adsorption rate was enhanced.

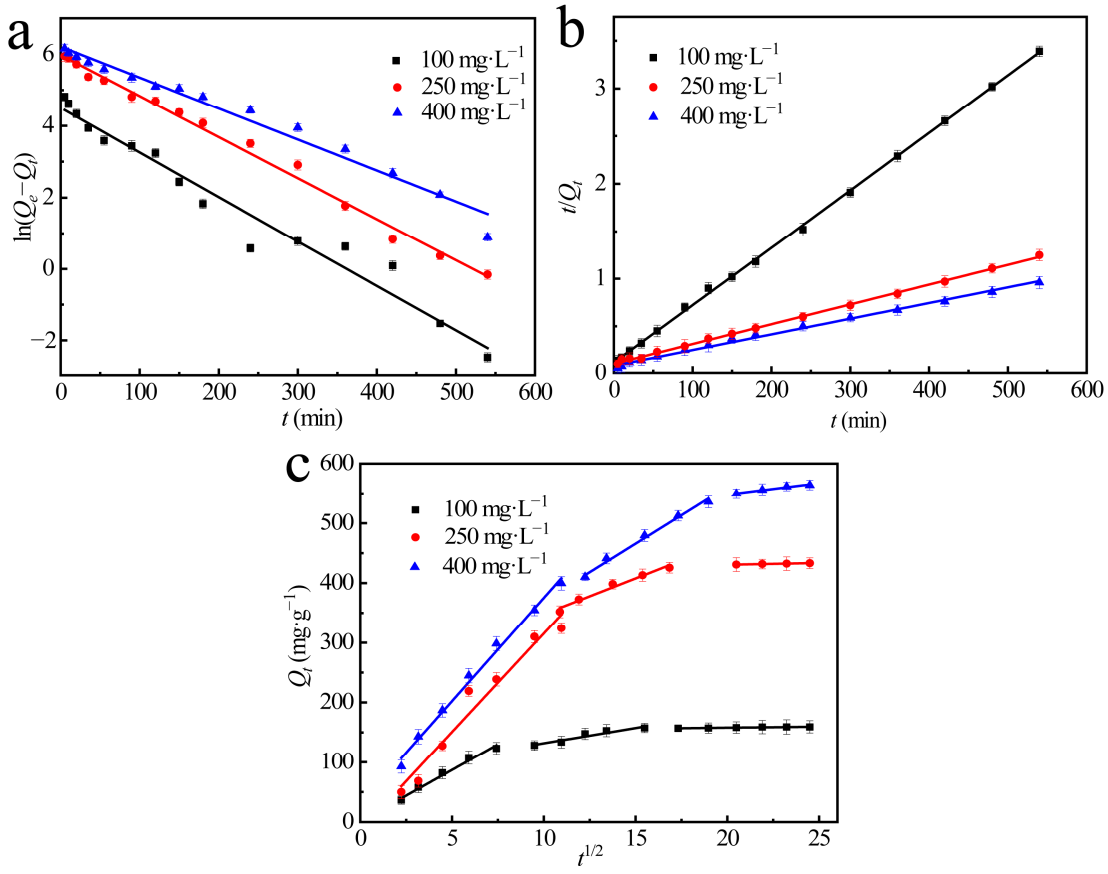

Figure 7. Fitting of (**a**) the pseudo-first-order, (**b**) the pseudo-second-order plots and (**c**) the intra-particle diffusion models for TC adsorption by MM3 (m_{MM3} = 0.01 g; pH = 4; V = 20 mL; T = 298 K; t = 12 h).

Table 2. Parameters of pseudo-first-order and pseudo-second-order kinetic models for the adsorption of TC by MM3.

Q_{exp} mg·g^{-1}	C_0 mg·L^{-1}	The Pseudo-First-Order Kinetic Model			The Pseudo-Second-Order Kinetic Model		
		k_1 min^{-1}	Q_e mg·g^{-1}	R^2	k_2 g·(mg·min)$^{-1}$	Q_e mg·g^{-1}	R^2
179.6	100	0.0123	90.3	0.966	3.03×10^{-4}	166.7	0.996
433.3	250	0.0115	394.7	0.992	0.46×10^{-4}	454.5	0.999
603.8	400	0.0080	498.7	0.977	0.32×10^{-4}	606.1	0.993

Table 3. Parameters of intra-particle diffusion model for the adsorption of TC onto MM.

C_0 mg·g^{-1}	The First Stage			The Second Stage			The Third Stage		
	k_{i1} mg·(g·min)$^{-1/2}$	C_{il}	R^2	k_{i2} mg·(g·min)$^{-1/2}$	C_{i2}	R^2	k_{i3} mg·(g·min)$^{-1/2}$	C_{i3}	R^2
100	17.16	1.2	0.981	5.10	80.8	0.917	0.35	151.0	0.947
250	32.94	0.3	0.949	10.68	229.0	0.961	0.57	419.4	0.993
400	34.56	29.5	0.992	19.03	180.4	0.990	3.77	472.9	0.956

Langmuir and Freundlich isotherm models were used to analyze the adsorption experimental data for further understanding the adsorption process, and the two isotherm models [49] are expressed as Equations (S4) and (S5).

In Table 4, the correlation coefficients of Langmuir models (R^2 = 0.988, 0.974 and 0.980) were greater than those of the Freundlich models (R^2 = 0.798, 0.797 and 0.897), and Q_m of Langmuir (657.9 mg·g^{-1}) was closer to actual the Q_e (645.8 mg·g^{-1}). This indicated that the adsorption of TC by the MM3 was a monolayer process [10]. The value of K_l became larger with rising temperature, suggesting that the adsorption of TC by the MM3 was an endothermic process. The parameter n in the Freundlich models represented the interaction intensity between the adsorbent material and pollutants, and the values of n were all greater than 2, suggesting that the adsorption of TC by MM proceeded easily [50–52]. Comparison of Q_m of the MM3 with other adsorbents is shown in Table 5. Q_m of the MM3 was much greater than that of MM0, zeolite, biochar, clay and modified ZIF-67, suggesting that the MM3 was a favorable competitor for the removal of TC from the water.

Table 4. The parameters of Langmuir and Freundlich adsorption isotherms of TC by MM3.

	T K	Q_e mg·g^{-1}	Langmuir			Freundlich		
			Q_m mg·g^{-1}	K_l·10^3 L·mg^{-1}	R^2	n	K_F (mg·g^{-1}) (L·mg^{-1})$^{-1/n}$	R^2
MM3	298	645.8	657.9	0.084	0.988	2.79	111.1	0.798
	308	701.4	719.42	0.115	0.974	2.85	128.3	0.797
	318	835.8	833.3	0.217	0.980	3.03	203.6	0.897
MM0	298	494.7	531.9	0.054	0.999	2.52	67.1	0.901

Table 5. Comparison of Q_m of TC by MM3 with other adsorbents.

Adsorbent	Q_m mg·g^{-1}	Reference
ZIF-67-immobilized WA (wood aerogel)	195.8	[53]
Hierarchical porous ZIF-8	976.8	[9]
Zeolite A–modified MCM-41	419.3	[54]
Montmorillonite	269.0	[17]
Biochar prepared from pine bark	58.5	[8]
$MnFe_2O_4$ rGO	41.0	[49]
MM0	386.9	This work
MM3	445.0	This work

3.5. Adsorption Thermodynamics

Adsorption thermodynamics can determine whether the adsorption is spontaneous. The adsorption process of TC by the MM3 (at 298, 308 and 318 K) was used to analyze the adsorption thermodynamics parameters. The thermodynamic parameters were obtained according to Equations (S6)–(S8) [55] and are shown in Table 6.

Table 6. The parameters of adsorption thermodynamics for the adsorption of TC by MM3.

T K	Q_e mg·g^{-1}	ΔG KJ·mol^{-1}	ΔH KJ·mol^{-1}	ΔS J·(mol·K)$^{-1}$
298	645.8	−8.83		
308	701.4	−10.37	37.24	154.58
318	835.8	−11.92		

From Table 6, the positive value of ΔH (37.24 KJ·mol^{-1}) confirmed that the TC adsorption onto the MM3 was an endothermic process. The positive value of ΔS (154.58 J·(mol·K)$^{-1}$) indicated that the system was getting messier after the TC adsorption [9]. The negative value of ΔG displayed that the adsorption of TC onto the MM3 was spontaneous and the higher temperature was beneficial to the TC adsorption and improved Q_e, which was identical with the results of the adsorption experiment.

3.6. Adsorption Performance in Salt Solution of MM3

TC coexists with inorganic salts in many real wastewaters. Therefore, the influence of different salt concentrations from saline water on the adsorption type of the TC by the MM3 was studied, as shown in Figure 8a. According to the literature, different concentrations of NaCl or Na_2SO_4 were added to prepare simulated wastewater [56]. Figure 8a displays that the Q_e of the TC by the MM3 were not reduced in a mixed solution of NaCl and TC but slightly higher than that in pure TC solution. The NaCl concentration increased to 5% and the Q_e rose from 440.1 to 463.0 mg·g^{-1}. The increased adsorption of tetracycline onto the adsorbents could be due to the decrease in solubility of the drug in the salt solution, commonly characterized as the salting-out effect [57]. The Na^+, SO_4^{2-} and Cl^- ions from the dissociation of NaCl and Na_2SO_4 in water were strongly solvated by the water molecules, forming large hydration spheres. These water molecules restricted mobility and are less able to interact with tetracycline molecules. Therefore, the solubility of tetracycline in the solution decreases, and its diffusion towards the adsorbent surface is favored, so the Q_e of the TC onto the MM3 increased [58]. As the concentration of Na_2SO_4 increased, the Q_e slightly decreased, which indicated that the existence of Na_2SO_4 had a negative influence on the TC adsorption. It was likely that the charge of SO_4^{2-} was greater than that of Cl^-, resulting in the stronger electrostatic interaction between the MM3 and the ions and affected the TC adsorption by the MM3 [59]. When NaCl and Na_2SO_4 were both present, the Q_e did not change significantly. The above results indicate that the MM3 still had a good adsorption capacity for the TC coexisting with salt, and could be used as a potential adsorbent for treating TC from saline water.

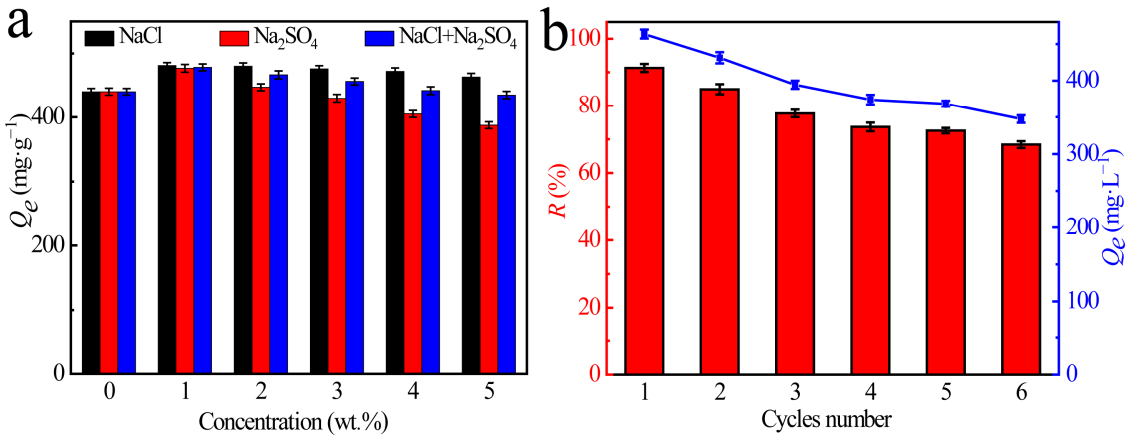

Figure 8. (**a**) Effect of inorganic salt concentration on the Q_e of MM3. (**b**) The regeneration performance of MM3 (m_{MM3} = 0.01 g; pH = 4; V = 20 mL; T = 298 K; C_0 = 250 mg·L^{-1}; t = 12 h).

3.7. Regeneration Performance of MM3

Regeneration performance is important to the practical application of adsorbents. The regeneration performance of the MM3 is shown in Figure 8b. NaOH solution with pH = 9 was selected as the eluent to make the TC desorb from the MM3 on account of strong electrostatic repulsion between the negatively charged MM3 and negatively charged TC molecules at pH = 9. The MM3 (0.01 g) remained inside the flask after TC adsorption and then added 20 mL pH = 9 NaOH was added. The flask was shaken at a set speed of 200 r·min^{-1} and temperature of 25 °C in an air shaker for 6 h and replaced with new lye at the time of 3 h. Then, the microspheres were washed with 20 mL deionized water for 2 h under the same conditions in the air shaker and dried for the next adsorption experiment. After the fifth cycle, the R of TC by the MM3 still reached 72.5%, and Q_e was reduced to 368.4 mg·g^{-1}, which was still much better than the Q_e of some adsorbents reported [53]. The results manifested that the MM3 are a promising green adsorbent with exceptional regeneration performance.

3.8. Column Studies

The impact of bed height on the breakthrough curves of TC was investigated, as shown in Figure 9, and the parameters were calculated as Equations (S9)–(S13) [60] and are given in Table 7. Notably, the breakthrough time, depletion time and Y all increased with rising bed height, but the Q_f decreased. The rise in bed height meant the increase in the amount of adsorbent in the fixed bed, which had more adsorption active sites, so the breakthrough time was prolonged and Y was increased. However, when there were too many active sites for adsorption, they could not all be fully utilized, resulting in a decrease in adsorption capacity [61,62].

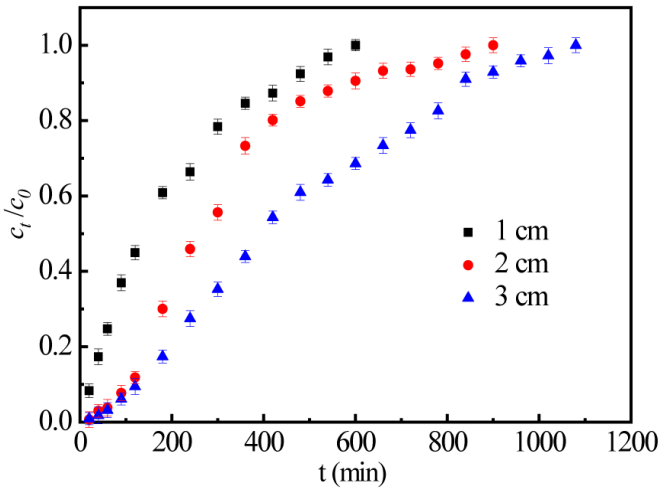

Figure 9. Effect of bed height on the breakthrough curves on TC adsporption by MM3 (pH = 4; T = 298 K; C_0 = 250 mg·L^{-1}; pH = 4).

Table 7. Parameters of the breakthrough curves of TC adsroption onto MM3.

Column Height Z cm	Adsorption Capacity Q_f mg·g^{-1}	Removal Efficiency Y %	Breakthrough Time t_b min	Saturation Time t_s min
1	783.79	31.35	40	480
2	633.10	33.77	120	600
3	629.39	41.96	180	840

Fitting curve and parameters of the Thomas and Yoon–Nelson models under different bed heights are shown in Figure S2 and Table 8, respectively. The values of k_{th} and k_{yn} decreased, and τ increased with increasing bed height because the rise in bed height caused an increment in flow resistance and a slower reaction rate [38]. Moreover, the higher bed height extended the residence time of the TC in the column, and the fuller contact between the TC and the MM3 made the adsorption performance better [63]. As a result, the prepared MM3 was not only economic and green but also could be conveniently carried out in fixed-bed columns for the continuous treatment of TC wastewater.

Table 8. Parameters of the breakthrough curves of TC adsroption onto MM3.

Column Height Z cm	Thomas Model			Yoon–Nelson		
	k_{th} L·(g·min)$^{-1}$	Q_f mg·g^{-1}	R^2	k_{yn} L·(g·min)$^{-1}$	τ min	R^2
1	0.03776	763.3	0.950	0.00944	183.2	0.950
2	0.03612	744.4	0.902	0.00903	357.3	0.902
3	0.02772	679.8	0.938	0.00693	489.5	0.938

3.9. Proposed Adsorption Mechanism

(i). Van der Waals forces and electrostatic interations

The Van der Waals force is a universal attraction between molecules and is deeply influenced by the specific area and pores of the adsorbents, which were correlated with adsorption capacity [53]. As shown above, the specific surface area of the MM3 became enlarged with the addition of oleic acid, leding to the increasing adsorption capacity of for TC, which might be caused by Van der Waals forces.

Electrostatic interaction were explained in great detail regarding the effect of pH value (Section 3.3.1). The adsorption capacity of TC by the MM3 at pH = 4 was the largest due to electrostatic attraction (the MM3 and TC were oppositely charged). It indicated that electrostatic interactions might contribute to the adsorption of TC.

(ii). Hydrogen–bonding interactions and ion exchange

In order to analyze hydrogen–bonding interactions and ion exchange between the MM3 and TC, FT-IR and XPS spectra of the MM3 before and after the TC adsorption were measured.

In Figure 10a, compared with the MM3, the new peaks of $–CH_3$ (1386 cm^{-1}) and $–CH_2$ (1490 cm^{-1}) were appeared in the TC@MM3, proving the presence of TC on the MM3. The peak of –OH was shifted from 1636 cm^{-1} in the MM3 to 1632 cm^{-1} in the TC@MM3, and the –C=O/C–O from the oleic acid was shifted from 1466 cm^{-1} in the MM3 to 1453 cm^{-1} in the TC@MM3, which might be due to hydrogen bonds between the TC and the geopolymer [9,18,64].

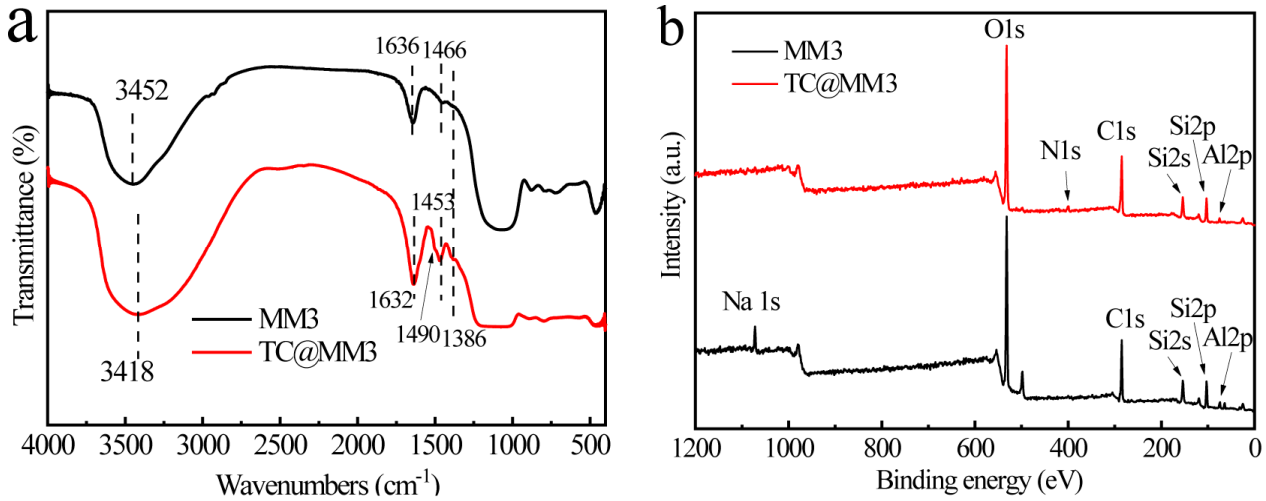

Figure 10. (**a**) FT-IR spectra of MM3 and (**b**) XPS total spectum of samples.

The peaks of Al 2p, Si 2p, O 1s, and C 1s (74.07, 102.37, 531.61 and 284.6 eV, respectively) in the MM3 and Al 2p, Si 2p, O 1s, and C 1s (74.34, 102.56, 531.86 and 284.6 eV, respectively) in the TC@MM3 were all observed in the XPS spectrum. The binding energy of O 1s was shifted to the higher value demonstrating the existence of weak interaction, including hydrogen bonding, Van der Waals forces, and electrostatic interactions [12,59]. The element composition of the MM3 and the TC@MM3 are displayed in Table S2. After the MM3 adsorbed the TC, the carbon content increased from 33.37% to 38.16%, and a new peak of N 1s (399.73 eV) was observed in the TC@MM3, suggesting the successful adsorption of TC on the MM3.

On the other hand, the Na 1s peak (1072 eV) in the MM3 disappeared after the TC adsorption. The occurrance of ion exchange in the adsorption process was confirmed. With the variation of pH, TC could undergo protonation–deprotonation transitions. The chemical species of TC included TC_2^+ at pH = 4 and TC_3^+ at low pH [17]. Na^+ was balanced with the negatively charged aluminum oxide tetrahedron $[AlO_4]^-$ in the geopolymer, which could

be ion exchanged with TC_2^+ and TC_3^+. Therefore, the TC_2^+ and TC_3^+ could be adsorbed on the MM3.

In conclusion, the adsorption mechanism of the MM3 for TC included Van der Waals forces, electrostatic interactions, hydrogen–bonding interactions, and ion exchange, as shown in Figure 11.

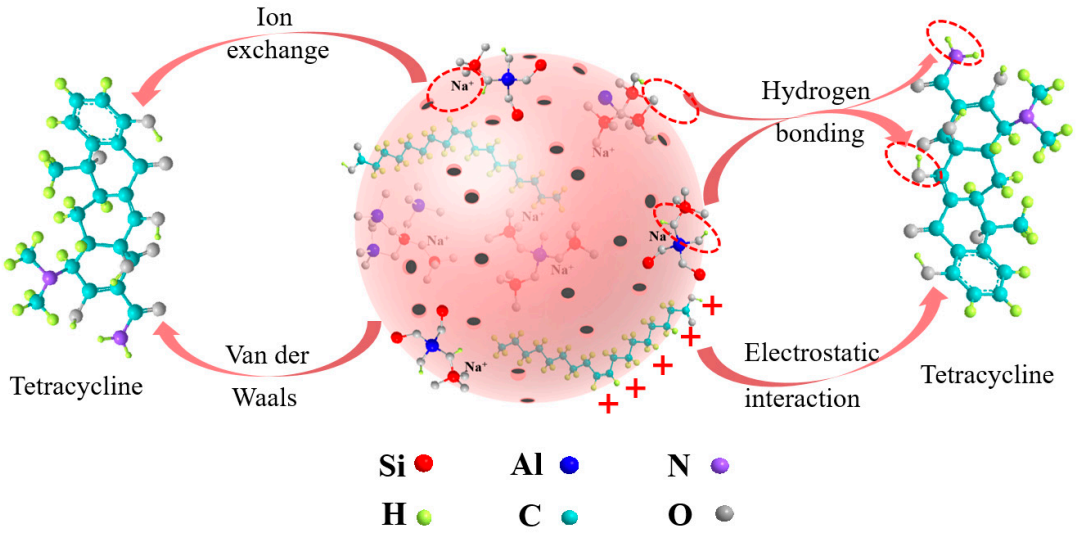

Figure 11. The proposed adsorption mechanism of TC by MM3.

4. Conclusions

In this study, metakaolin-based geopolymer microspheres modified by oleic acid were successfully prepared to enhance adsorption of tetracycline in an aqueous solution. The structure and adsorption performance of the MM were systematically adjusted by changing the dosage of the oleic acid. The MM3 with the 0.03% oleic acid addition had the largest specific surface area and pore volume as well as the highest Q_e for TC. The pseudo-second-order kinetic and Langmuir isotherm models were fitted to describe the adsorption process. The Langmuir adsorption capacity of TC by the MM3 reached 657.9 $mg \cdot g^{-1}$ at 298 K. Thermodynamic study showed that the TC adsorption onto the MM3 was a spontaneous and endothermic process. The adsorption performance of the MM3 for TC from saline water was shown to be stable, and even slightly increased in NaCl solution. After the fifth cycle, the Q_e still reached 368.4 $mg \cdot g^{-1}$. The fixed-bed tests indicated that the MM3 effectively and continuously adsorbed TC from water, and the Thomas and Yoon–Nelson models could account for the TC adsorption in a fixed-bed system. Based on the experimental results and various characterizations, the adsorption mechanism of the MM3 for TC involved Van der Waals forces, hydrogen bonding, electrostatic interactions, and ion exchange. In short, the MM3 has the advantages of low price, environmental friendliness and simple preparation and showed good application prospects in the removal of TC from actual wastewater.

Supplementary Materials: The following supporting information can be downloaded at: https://www.mdpi.com/article/10.3390/su14116705/s1, Figure S1: (a) Langmuir and (b) Freundlich adsorption isotherms (m_{MM3} = 0.01 g; pH = 4; V = 20 ml; t = 12 h); Figure S2: Linear plots of (a) Thomas and (b) Yoon-Nelson model. Table S1: Porosity parameters of MM with different dosage of oleic acid; Table S2: The element composition in XPS.

Author Contributions: Conceptualization, X.W.; Funding acquisition, Y.G.; Software, Z.Z.; Writing—original draft, X.W. All authors have read and agreed to the published version of the manuscript.

Funding: This work was supported by the National Natural Science Foundation of China (21707022) and the Guangxi Natural Science Foundation (2020GXNSFAA159039, AD21220012).

Institutional Review Board Statement: Not applicable.

Informed Consent Statement: Not applicable.

Conflicts of Interest: The authors declare no conflict of interest.

References

1. Imran, M.; Das, K.R.; Naik, M.M. Co-selection of multi-antibiotic resistance in bacterial pathogens in metal and microplastic contaminated environments: An emerging health threat. *Chemosphere* **2019**, *215*, 846–857. [CrossRef] [PubMed]
2. Xu, J.; Xu, Y.; Wang, H.; Guo, C.; Qiu, H.; He, Y.; Zhang, Y.; Li, X.; Meng, W. Occurrence of antibiotics and antibiotic resistance genes in a sewage treatment plant and its effluent-receiving river. *Chemosphere* **2015**, *119*, 1379–1385. [CrossRef] [PubMed]
3. Luo, Y.; Xu, L.; Rysz, M.; Wang, Y.; Zhang, H.; Alvarez, P.J.J. Occurrence and Transport of Tetracycline, Sulfonamide, Quinolone, and Macrolide Antibiotics in the Haihe River Basin, China. *Environ. Sci. Technol.* **2011**, *45*, 1827–1833. [CrossRef] [PubMed]
4. Xu, L.; Zhang, H.; Xiong, P.; Zhu, Q.; Liao, C.; Jiang, G. Occurrence, fate, and risk assessment of typical tetracycline antibiotics in the aquatic environment: A review. *Sci. Total Environ.* **2021**, *753*, 141975. [CrossRef] [PubMed]
5. Yuan, F.; Hu, C.; Hu, X.; Wei, D.; Chen, Y.; Qu, J. Photodegradation and toxicity changes of antibiotics in UV and UV/H2O2 process. *J. Hazard. Mater.* **2011**, *185*, 1256–1263. [CrossRef] [PubMed]
6. Dai, Y.; Liu, M.; Li, J.; Yang, S.; Sun, Y.; Sun, Q.; Wang, W.; Lu, L.; Zhang, K.; Xu, J.; et al. A review on pollution situation and treatment methods of tetracycline in groundwater. *Sep. Sci. Technol.* **2019**, *55*, 1005–1021. [CrossRef]
7. Ahmad, F.; Zhu, D.; Sun, J. Environmental fate of tetracycline antibiotics: Degradation pathway mechanisms, challenges, and perspectives. *Environ. Sci. Eur.* **2021**, *33*, 64. [CrossRef]
8. Naghipour, D.; Hoseinzadeh, L.; Taghavi, K.; Jaafari, J.; Amouei, A. Effective removal of tetracycline from aqueous solution using biochar prepared from pine bark: Isotherms, kinetics and thermodynamic analyses. *Int. J. Environ. Anal. Chem.* **2021**, *11*, 1–14. [CrossRef]
9. Zhang, Z.; Chen, Y.; Hu, C.; Zuo, C.; Wang, P.; Chen, W.; Ao, T. Efficient removal of tetracycline by a hierarchically porous ZIF-8 metal organic framework. *Environ. Res.* **2021**, *198*, 111254. [CrossRef]
10. Qu, J.; Wang, S.; Jin, L.; Liu, Y.; Yin, R.; Jiang, Z.; Tao, Y.; Huang, J.; Zhang, Y. Magnetic porous biochar with high specific surface area derived from microwave-assisted hydrothermal and pyrolysis treatments of water hyacinth for Cr(VI) and tetracycline adsorption from water. *Bioresour. Technol.* **2021**, *340*, 125692. [CrossRef]
11. Li, B.; Huang, Y.; Wang, Z.; Li, J.; Liu, Z.; Fan, S. Enhanced adsorption capacity of tetracycline on tea waste biochar with KHCO3 activation from aqueous solution. *Environ. Sci. Pollut. Res.* **2021**, *28*, 44140–44151. [CrossRef] [PubMed]
12. Wang, P.; Tian, Y.; Wang, H.; Zhang, J.; Kong, L.; Zuo, W.; Li, D.; Yin, L. Strong adsorption of tetracycline on octahedral Cu2O nanocrystals exposed with {111} facets: Adsorption behavior and mechanism insight. *Appl. Surf. Sci.* **2021**, *542*, 148545. [CrossRef]
13. Tanyol, M.; Torğut, G. Chitosan-graft-poly(N-tert-butylacrylamide) Copolymer: Synthesis, Characterization and Optimization of Tetracycline Removal Using RSM. *J. Polym. Environ.* **2021**, *30*, 752–764. [CrossRef]
14. Nasiri, A.; Malakootian, M.; Shiri, M.A.; Yazdanpanah, G.; Nozari, M. CoFe2O4@methylcellulose synthesized as a new magnetic nanocomposite to tetracycline adsorption: Modeling, analysis, and optimization by response surface methodology. *J. Polym. Res.* **2021**, *28*, 192. [CrossRef]
15. Zhang, G.; Wo, R.; Sun, Z.; Hao, G.; Liu, G.; Zhang, Y.; Guo, H.; Jiang, W. Effective Magnetic MOFs Adsorbent for the Removal of Bisphenol A, Tetracycline, Congo Red and Methylene Blue Pollutions. *Nanomaterials* **2021**, *11*, 1917. [CrossRef]
16. Chen, B.; Li, Y.; Li, M.; Cui, M.; Xu, W.; Li, L.; Sun, Y.; Wang, M.; Zhang, Y.; Chen, K. Rapid adsorption of tetracycline in aqueous solution by using MOF-525/graphene oxide composite. *Microporous Mesoporous Mater.* **2021**, *328*, 111457. [CrossRef]
17. Zhang, H.; Shi, M.; Xia, M.; Wang, F.; Zhao, F. The Adsorption Mechanism of Montmorillonite for Different Tetracycline Species at Different pH Conditions: The Novel Visual Analysis of Intermolecular Interactions. *Water Air Soil Pollut.* **2021**, *232*, 65. [CrossRef]
18. Chang, P.-H.; Jean, J.-S.; Jiang, W.-T.; Li, Z. Mechanism of tetracycline sorption on rectorite. *Colloids Surf. A Physicochem. Eng. Asp.* **2009**, *339*, 94–99. [CrossRef]
19. Rasaki, S.A.; Bingxue, Z.; Guarecuco, R.; Thomas, T.; Minghui, Y. Geopolymer for use in heavy metals adsorption, and advanced oxidative processes: A critical review. *J. Clean. Prod.* **2019**, *213*, 42–58. [CrossRef]
20. Villaquirán Caicedo, M.A.; Gutiérrez, R.M.D. Synthesis of ternary geopolymers based on metakaolin, boiler slag and rice husk ash. *Dyna* **2015**, *82*, 104–110. [CrossRef]
21. Ma, S.; Fu, S.; Zhao, S.; He, P.; Ma, G.; Wang, M.; Jia, D.; Zhou, Y. Direct ink writing of geopolymer with high spatial resolution and tunable mechanical properties. *Addit. Manuf.* **2021**, *46*, 102202. [CrossRef]
22. Siyal, A.A.; Shamsuddin, M.R.; Khan, M.I.; Rabat, N.E.; Zulfiqar, M.; Man, Z.; Siame, J.; Azizli, K.A. A review on geopolymers as emerging materials for the adsorption of heavy metals and dyes. *J. Environ. Manag.* **2018**, *224*, 327–339. [CrossRef] [PubMed]
23. He, P.; Zhang, Y.; Zhang, X.; Chen, H. Diverse zeolites derived from a circulating fluidized bed fly ash based geopolymer for the adsorption of lead ions from wastewater. *J. Clean. Prod.* **2021**, *312*, 127769. [CrossRef]
24. Salam, M.A.; Mokhtar, M.; Albukhari, S.M.; Baamer, D.F.; Palmisano, L.; Abukhadra, M.R. Insight into the role of the zeolitization process in enhancing the adsorption performance of kaolinite/diatomite geopolymer for effective retention of Sr (II) ions; batch and column studies. *J. Environ. Manag.* **2021**, *294*, 112984. [CrossRef]
25. Siyal, A.A.; Shamsuddin, M.R.; Khahro, S.H.; Low, A.; Ayoub, M. Optimization of synthesis of geopolymer adsorbent for the effective removal of anionic surfactant from aqueous solution. *J. Environ. Chem. Eng.* **2021**, *9*, 104949. [CrossRef]

26. Tome, S.; Hermann, D.T.; Shikuku, V.O.; Otieno, S. Synthesis, characterization and application of acid and alkaline activated volcanic ash-based geopolymers for adsorptive remotion of cationic and anionic dyes from water. *Ceram. Int.* **2021**, *47*, 20965–20973. [CrossRef]
27. He, P.; Wang, Q.; Fu, S.; Wang, M.; Zhao, S.; Liu, X.; Jiang, Y.; Jia, D.; Zhou, Y. Hydrothermal transformation of geopolymers to bulk zeolite structures for efficient hazardous elements adsorption. *Sci. Total Environ.* **2021**, *767*, 144973. [CrossRef]
28. Zhang, J.; Ge, Y.; Li, Z.; Wang, Y. Facile fabrication of a low-cost and environmentally friendly inorganic-organic composite membrane for aquatic dye removal. *J. Environ. Manag.* **2020**, *256*, 109969. [CrossRef]
29. Kutuniva, J.; Mäkinen, J.; Kauppila, T.; Karppinen, A.; Hellsten, S.; Luukkonen, T.; Lassi, U. Geopolymers as active capping materials for in situ remediation of metal(loid)-contaminated lake sediments. *J. Environ. Chem. Eng.* **2019**, *7*, 102852. [CrossRef]
30. El Alouani, M.; Saufi, H.; Moutaoukil, G.; Alehyen, S.; Nematollahi, B.; Belmaghraoui, W.; Taibi, M. Application of geopolymers for treatment of water contaminated with organic and inorganic pollutants: State-of-the-art review. *J. Environ. Chem. Eng.* **2021**, *9*, 105095. [CrossRef]
31. Tang, Q.; Ge, Y.-Y.; Wang, K.-T.; He, Y.; Cui, X.-M. Preparation and characterization of porous metakaolin-based inorganic polymer spheres as an adsorbent. *Mater. Des.* **2015**, *88*, 1244–1249. [CrossRef]
32. Papa, E.; Mor, M.; Murri, A.N.; Landi, E.; Medri, V. Ice-templated geopolymer beads for dye removal. *J. Colloid Interface Sci.* **2020**, *572*, 364–373. [CrossRef] [PubMed]
33. Liu, Y.; Yan, C.; Zhang, Z.; Li, L.; Wang, H.; Pu, S. One-step fabrication of novel porous and permeable self-supporting zeolite block from fly ash. *Mater. Lett.* **2017**, *196*, 328–331. [CrossRef]
34. Li, F.; Chen, L.; Chen, W.; Bao, Y.; Zheng, Y.; Huang, B.; Mu, Q.; Wen, D.; Feng, C. Antibiotics in coastal water and sediments of the East China Sea: Distribution, ecological risk assessment and indicators screening. *Mar. Pollut. Bull.* **2020**, *151*, 110810. [CrossRef]
35. Zaidi, F.H.A.; Ahmad, R.; Abdullah, M.M.A.B.; Rahim, S.Z.A.; Yahya, Z.; Li, L.Y.; Ediati, R. Geopolymer as underwater concreting material: A review. *Constr. Build. Mater.* **2021**, *291*, 123276. [CrossRef]
36. Su, Q.; Deng, L.; Ye, Q.; He, Y.; Cui, X. KOH-Activated Geopolymer Microspheres Recycle Co(II) with Higher Adsorption Capacity than NaOH-Activated Ones. *ACS Omega* **2020**, *5*, 23898–23908. [CrossRef]
37. Abukhadra, M.R.; Dardir, F.M.; Ahmed, E.A.; Soliman, M.F. Efficient removal of Sr ions from water utilizing a novel Ni-/Fe-doped spongy apatite through fixed bed column system: Optimization and realistic application. *Clean Technol. Environ. Policy* **2018**, *21*, 69–80. [CrossRef]
38. Mostafa, M.; Bin Jumah, M.N.; Othman, S.I.; Alruhaimi, R.S.; Salama, Y.F.; Allam, A.A.; Abukhadra, M.R. Effective removal of different species of organophosphorus pesticides (acephate, omthosate, and methyl parathion) using chitosan/Zeolite-A as multifunctional adsorbent. *Environ. Technol. Innov.* **2021**, *24*, 101875. [CrossRef]
39. Ozer, I.; Soyer-Uzun, S. Relations between the structural characteristics and compressive strength in metakaolin based geopolymers with different molar Si/Al ratios. *Ceram. Int.* **2015**, *41*, 10192–10198. [CrossRef]
40. Liu, Y.; Yan, C.; Zhang, Z.; Gong, Y.; Wang, H.; Qiu, X. A facile method for preparation of floatable and permeable fly ash-based geopolymer block. *Mater. Lett.* **2016**, *185*, 370–373. [CrossRef]
41. Qiu, Y.; Kong, L.; Chen, T.; Xu, Q. Efficient Adsorption of Tetracycline Using Cu+-Modified SBA-15 and Its Adsorption Mechanism. *J. Environ. Eng.* **2021**, *147*, 04020142. [CrossRef]
42. Yuan, M.; Li, C.; Zhang, B.; Wang, J.; Zhu, J.; Ji, J.; Ma, Y. A mild and one-pot method to activate lignin-derived biomass by using boric acid for aqueous tetracycline antibiotics removal in water. *Chemosphere* **2021**, *280*, 130877. [CrossRef] [PubMed]
43. Gu, C.; Karthikeyan, K.G. Interaction of tetracycline with aluminum and iron hydrous oxides. *Environ. Sci. Technol.* **2005**, *39*, 2660–2667. [CrossRef] [PubMed]
44. Qu, J.; Liu, Y.; Cheng, L.; Jiang, Z.; Zhang, G.; Deng, F.; Wang, L.; Han, W.; Zhang, Y. Green synthesis of hydrophilic activated carbon supported sulfide nZVI for enhanced Pb(II) scavenging from water: Characterization, kinetics, isotherms and mechanisms. *J. Hazard. Mater.* **2021**, *403*, 123607. [CrossRef] [PubMed]
45. Ghorai, S.; Sarkar, A.K.; Panda, A.B.; Pal, S. Effective removal of Congo red dye from aqueous solution using modified xanthan gum/silica hybrid nanocomposite as adsorbent. *Bioresour. Technol.* **2013**, *144*, 485–491. [CrossRef]
46. Agarwal, S.; Pramanick, S.; Rahaman, S.A.; Ghanta, K.C.; Dutta, S. A cost-effective approach for abatement of cyanide using iron-impregnated activated carbon: Kinetic and equilibrium study. *Appl. Water Sci.* **2019**, *9*, 74. [CrossRef]
47. Yan, S.; He, P.; Jia, D.; Wang, Q.; Liu, J.; Yang, J.; Huang, Y. Synthesis of novel low-cost porous gangue microsphere/geopolymer composites and their adsorption properties for dyes. *Int. J. Appl. Ceram. Technol.* **2018**, *15*, 1602–1614. [CrossRef]
48. Teong, C.Q.; Setiabudi, H.D.; El-Arish, N.A.S.; Bahari, M.B.; Teh, L.P. Vatica rassak wood waste-derived activated carbon for effective Pb(II) adsorption: Kinetic, isotherm and reusability studies. *Mater. Today Proc.* **2021**, *42*, 165–171. [CrossRef]
49. Bao, J.; Zhu, Y.; Yuan, S.; Wang, F.; Tang, H.; Bao, Z.; Zhou, H.; Chen, Y. Adsorption of Tetracycline with Reduced Graphene Oxide Decorated with $MnFe_2O_4$ Nanoparticles. *Nanoscale Res. Lett.* **2018**, *13*, 396. [CrossRef]
50. Ahmed, S.; Rehman, H.U.; Ali, Z.; Qadeer, A.; Haseeb, A.; Ajmal, Z. Solvent assisted synthesis of hierarchical magnesium oxide flowers for adsorption of phosphate and methyl orange: Kinetic, isotherm, thermodynamic and removal mechanism. *Surfaces Interfaces* **2021**, *23*, 100953. [CrossRef]
51. Fang, Y.; Yang, K.; Zhang, Y.; Peng, C.; Robledo-Cabrera, A.; López-Valdivieso, A. Highly surface activated carbon to remove Cr(VI) from aqueous solution with adsorbent recycling. *Environ. Res.* **2021**, *197*, 111151. [CrossRef] [PubMed]

52. Ziyat, H.; Elmzioui, S.; Naciri Bennani, M.; Houssaini, J.; Allaoui, S.; Arhzaf, S. Kinetic, isotherm, and mechanism investigations of the removal of nitrate and nitrite from water by the synthesized hydrotalcite Mg–Al. *Res. Chem. Intermed.* **2021**, *47*, 2605–2627. [CrossRef]
53. Chen, G.; He, S.; Shi, G.; Ma, Y.; Ruan, C.; Jin, X.; Chen, Q.; Liu, X.; Dai, H.; Chen, X.; et al. In-situ immobilization of ZIF-67 on wood aerogel for effective removal of tetracycline from water. *Chem. Eng. J.* **2021**, *423*, 130184. [CrossRef]
54. Liu, M.; Hou, L.-A.; Yu, S.; Xi, B.; Zhao, Y.; Xia, X. MCM-41 impregnated with A zeolite precursor: Synthesis, characterization and tetracycline antibiotics removal from aqueous solution. *Chem. Eng. J.* **2013**, *223*, 678–687. [CrossRef]
55. Lima, E.C.; Hosseini-Bandegharaei, A.; Moreno-Piraján, J.C.; Anastopoulos, I. A critical review of the estimation of the thermodynamic parameters on adsorption equilibria. Wrong use of equilibrium constant in the Van't Hoof equation for calculation of thermodynamic parameters of adsorption. *J. Mol. Liq.* **2019**, *273*, 425–434. [CrossRef]
56. Srivastava, A.; Parida, V.K.; Majumder, A.; Gupta, B.; Gupta, A.K. Treatment of saline wastewater using physicochemical, biological, and hybrid processes: Insights into inhibition mechanisms, treatment efficiencies and performance enhancement. *J. Environ. Chem. Eng.* **2021**, *9*, 105775. [CrossRef]
57. Spaltro, A.; Pila, M.N.; Colasurdo, D.D.; Grau, E.N.; Román, G.; Simonetti, S.; Ruiz, D.L. Removal of paracetamol from aqueous solution by activated carbon and silica. Experimental and computational study. *J. Contam. Hydrol.* **2021**, *236*, 103739. [CrossRef]
58. Igwegbe, C.A.; Aniagor, C.O.; Oba, S.N.; Yap, P.-S.; Iwuchukwu, F.U.; Liu, T.; de Souza, E.C.; Ighalo, J.O. Environmental protection by the adsorptive elimination of acetaminophen from water: A comprehensive review. *J. Ind. Eng. Chem.* **2021**, *104*, 117–135. [CrossRef]
59. Liao, Q.; Rong, H.; Zhao, M.; Luo, H.; Chu, Z.; Wang, R. Strong adsorption properties and mechanism of action with regard to tetracycline adsorption of double-network polyvinyl alcohol-copper alginate gel beads. *J. Hazard. Mater.* **2021**, *422*, 126863. [CrossRef]
60. Mohanta, S.; Sahu, M.K.; Mishra, P.C.; Giri, A.K. Removal of Cr (VI) from aqueous solution by activated charcoal derived from Sapindus trifoliate L fruit biomass using continuous fixed bed column studies. *Water Sci. Technol.* **2021**, *84*, 55–65. [CrossRef]
61. Lin, X.; Huang, Q.; Qi, G.; Shi, S.; Xiong, L.; Huang, C.; Chen, X.; Li, H.; Chen, X. Estimation of fixed-bed column parameters and mathematical modeling of breakthrough behaviors for adsorption of levulinic acid from aqueous solution using SY-01 resin. *Sep. Purif. Technol.* **2017**, *174*, 222–231. [CrossRef]
62. Nazari, G.; Abolghasemi, H.; Esmaieli, M.; Pouya, E.S. Aqueous phase adsorption of cephalexin by walnut shell-based activated carbon: A fixed-bed column study. *Appl. Surf. Sci.* **2016**, *375*, 144–153. [CrossRef]
63. Ge, Y.; Cui, X.; Liao, C.; Li, Z. Facile fabrication of green geopolymer/alginate hybrid spheres for efficient removal of Cu(II) in water: Batch and column studies. *Chem. Eng. J.* **2017**, *311*, 126–134. [CrossRef]
64. Porubcan, L.S.; Serna, C.J.; White, J.L.; Hem, S.L. Mechanism of Adsorption of Clindamycin and Tetracycline by Montmorillonite. *J. Pharm. Sci.* **1978**, *67*, 1081–1087. [CrossRef] [PubMed]